Journal of Hydroscience and Hydraulic Engineering
Vol. 22, No.2 November, 2004, 11-24

NUMERICAL SIMULATION OF COMPLEX FLOW OVER BACKWARD-FACING STEP

By

Yuki Kajikawa
Masanori Michiue
Yuhei Matsubara
Osamu Hinokidani

Tottori University, Tottori, Japan

and

Hidetoshi Nakamoto

Tokyo Construction Consultants Co., Ltd., Osaka, Japan

SYNOPSIS

When a flow over backward-facing step or consolidation work includes both subcritical and supercritical flows, a wave jump or a submerged jet forms in the flow field. In the case of a movable bed, each flow generates a very complicated local scouring at the downstream of these structures, and this local scouring decreases the stability of these structures. Therefore, it is a very important to predict this complex flow. In this paper, we present a 2-dimensional vertical numerical model which can reproduce such complex flow over backward-facing step as the premise model which can reproduce local scouring. The numerical model is based on the MacCormack scheme, and the Favor method is introduced into the basic equations. The velocities, water depth, and non-static pressure are computed. The numerical results are in good agreement with the experimental ones for the waver jump, submerged jet, and shift process of each flow.

INTRODUCTION

When a flow over backward-facing step or consolidation work includes both subcritical and supercritical flows, a wave jump or a submerged jet forms in the flow field. The wave jump is in the state of a flow in which the main flow after leaving the step flows along the water surface and undulations propagate far downstream (see Photo. 1), and the submerged jet is in the state of a flow in which the main flow after leaving the step flows along the channel bed and the roller of reverse flow is formed near the water surface (see Photo. 2). It is known that a wave jump forms when the difference of the water level between the upstream and downstream becomes small, and the submerged jet forms when it becomes large (see Suzuki et al. (12)).

In the case of a movable bed, each flow generates a very complicated local scouring; that is, when a submerged jet forms, a rapid local scouring occurs because of that the reattachment point position of the main flow is near the step (see Fig. 1). However, since the water level is raised by the dune which is formed in just downstream of the scouring hole simultaneously, the flow shifts to the wave jump. When the wave jump is formed, the reattachment point position of the main flow moves far from the step, and the dune returns to the scouring hole (see Fig. 2). However, since the water level falls gradually, the flow shifts to the submerged jet again. These phenomena occur repeatedly and thus local scouring advances.

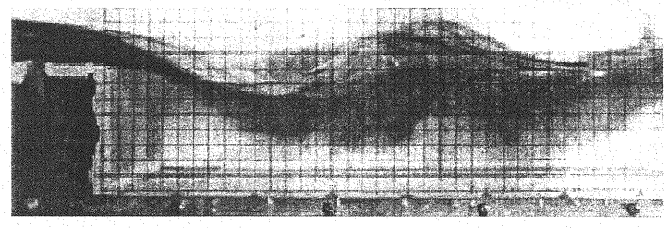

Photo. 1 Wave Jump

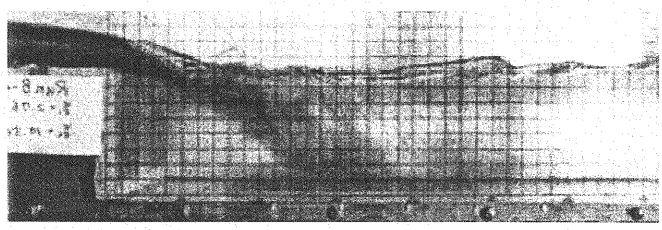

Photo. 2 Submerged Jet

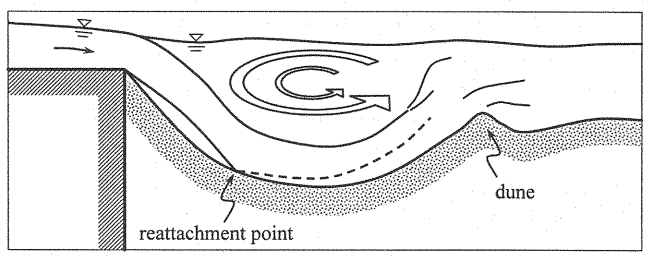

Fig. 1 Rapid scouring process by the submerged jet

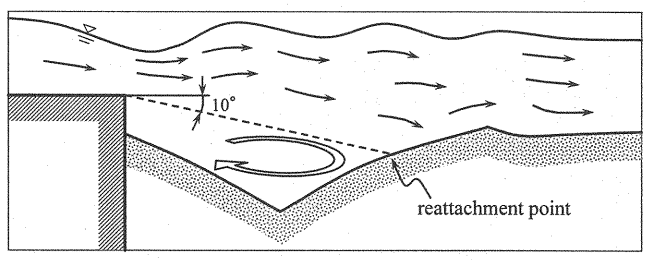

Fig. 2 Return process of scouring hole by the wave jump

Since the local scouring decreases the stability of these structures, it is a very important problem on disaster prevention. Therefore, many experimental investigations have been carried out hitherto about the characteristics of these flows (see Suzuki et al. (12); Ohtsu et al. (11); Kurniawan et al. (6)) and the prediction of the local scouring depth (see Kanda et al. (5); Michiue et al. (8)), and about characteristics of the complex flow over backward-facing step, the shift conditions of each flow (the wave jump and the submerged jet) has been examined in detail by Suzuki et al. (12).

When such a local scouring phenomenon is predicted analytically, it is necessary to reproduce that flow field correctly. Since a vertical direction flow is greater in the downstream of the step, it is necessary to analyze by a 2-dimensional vertical or 3-dimensional numerical model which reproduces also the shift process of each flow. Many numerical analyses for the flow over backward-facing step have been carried out (see Blom (1); Nakayama et al. (10)). However, investigations of numerical analysis for the flow which include both subcritical and supercritical flow are still scarce.

In this paper, we present a 2-dimensional vertical numerical model which can analyze accurately the complex flow over backward-facing step as the foundations of a model which can analyze the local scouring. The analysis object is the experiment of complex flow over back-ward facing step by Suzuki et al (12). In the numerical model, a 0-equation model which is a comparatively simple model is adapted to the Reynolds stress in consideration of bed evolution calculation at the next stage, and the Favor method (see Hirt et al. (3), (4)) is employed which has the ability to impose boundary conditions smoothly at complicated boundaries. Furthermore, the MacCormack explicit finite-difference scheme (see Liu (7)) is applied to the discretization of the governing equations.

NUMERICAL MODEL

Governing Equations

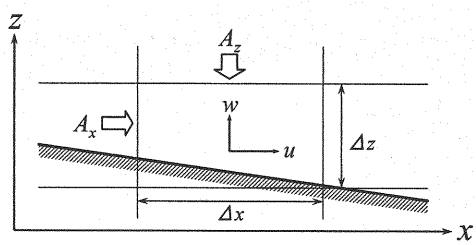

Fig. 3 Defined direction of fractional area

A well-used boundary fitted-coordinate system can produce the form of a river course or a river bed to the coordinate system itself and can easily yield a high degree of accuracy. However, much labor is involved in using various lattice forming methods; and if boundaries are more complicated, accuracy may decrease by calculating points set at dense or rough levels. Therefore, in this study, we adopt the Cartesian coordinate system, and the Favor method which has the ability to impose boundary conditions smoothly at complicated boundaries is introduced into the governing equations. In the Favor method, it is assumed that both fluid and boundary exist in an arbitrary lattice, if the volume fraction is occupied by fluid, the volume porosity of the flow region at an arbitrary point is V, if a fraction of area, the area porosity in a cross section perpendicular to the x-direction is A_x. The same is the case of the z-direction. For the defined direction of the fractional area, etc., shown in Fig. 3. Governing equations in a Cartesian coordinate compose of a 2-dimensional vertical continuity equation, momentum equations and a depth averaged 2-dimensional continuity equation introduced by the Favor method. They are denoted by the following equations:

[2-dimensional vertical continuity equation]

$$\frac{\partial}{\partial x}\left(A_x u\right)+\frac{\partial}{\partial z}\left(A_z w\right)=0 \tag{1}$$

[2-dimensional vertical momentum equation]

$$\frac{\partial u}{\partial t}+\frac{1}{V}\left\{\frac{\partial}{\partial x}\left(A_x u^2\right)+\frac{\partial}{\partial z}\left(A_z uw\right)\right\}=-\frac{1}{\rho}\frac{\partial p}{\partial x}+\frac{1}{V}\left\{\frac{\partial}{\partial x}\left(A_x \varepsilon_h \frac{\partial u}{\partial x}\right)+\frac{\partial}{\partial z}\left(A_z \varepsilon_z \frac{\partial u}{\partial z}\right)\right\} \tag{2}$$

$$\frac{\partial w}{\partial t}+\frac{1}{V}\left\{\frac{\partial}{\partial x}\left(A_x uw\right)+\frac{\partial}{\partial z}\left(A_z w^2\right)\right\}=-g-\frac{1}{\rho}\frac{\partial p}{\partial z}+\frac{1}{V}\left\{\frac{\partial}{\partial x}\left(A_x \varepsilon_h \frac{\partial w}{\partial x}\right)+\frac{\partial}{\partial z}\left(A_z \varepsilon_z \frac{\partial w}{\partial z}\right)\right\} \tag{3}$$

[Depth averaged continuity equation]

$$\frac{\partial h}{\partial t}+\frac{\partial}{\partial x}(\bar{u}h)=0 \tag{4}$$

where x, z = horizontal and vertical axis of the coordinate; u, w = velocity in the x- and y-direction; V = fractional volume; A_x, A_z = fractional area in the x- and z- direction; ρ = water density; g = gravity acceleration; p = pressure; ε_h, ε_z = eddy viscosity coefficient in the horizontal and vertical direction; h = flow depth; and the over bar $\bar{}$ denotes the depth averaged value. Thus, the eddy viscosity coefficient in the horizontal ε_h and vertical direction ε_z is evaluated by the following equations:

$$\varepsilon_h=\frac{1}{6}\kappa u_* h \;\; ; \quad \varepsilon_z=\kappa u_* z'\left(1-\frac{z'}{h}\right) \tag{5}$$

where κ = Von Karman constant (κ = 0.41); u_* = shear velocity; and z' = zero at the bed level and positive upper in the vertical direction.

Numerical Scheme

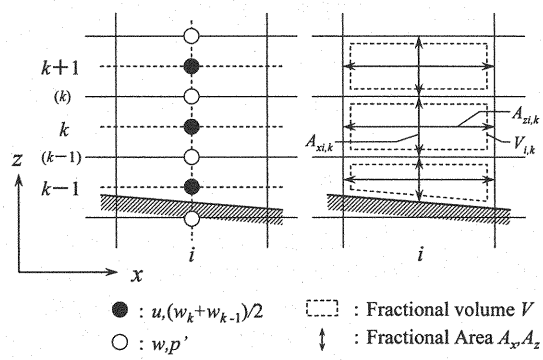

Fig. 4 Arrangement of calculating point

To Eqs. 2 and 4, we apply the MacCormack scheme which has been widely used in computational fluid dynamics to calculate u and h. The arrangement of calculating points is shown in Fig. 4. This scheme consists of a two-step predictor-corrector sequence and is applicable to the complex flow field. In order to control the numerical vibration by discretization error by means of this scheme, it is necessary to add an artificial viscosity term to the finite difference equations. The Eqs. 2 and 4 are denoted by the following equation in the matrix form of conservation:

$$\frac{\partial U}{\partial t}+\frac{1}{V}\left(\frac{\partial E}{\partial x}+\frac{\partial G}{\partial z}\right)=C \tag{6}$$

$$U=\begin{pmatrix}u\\h\end{pmatrix} \;\; ; \quad E=\begin{pmatrix}A_x u^2\\ \bar{u}h\end{pmatrix} \;\; ; \quad G=\begin{pmatrix}A_z uw\\0\end{pmatrix} \;\; ;$$

$$C=\begin{pmatrix}-\dfrac{1}{\rho}\dfrac{\partial p}{\partial x}+\dfrac{1}{V}\left\{\dfrac{\partial}{\partial x}\left(A_x\varepsilon_h\dfrac{\partial u}{\partial x}\right)+\dfrac{\partial}{\partial z}\left(A_z\varepsilon_z\dfrac{\partial u}{\partial z}\right)\right\}\\0\end{pmatrix}$$

where $V = 1.0$ in case of the depth averaged continuity equation (Eq. 4).

In the MacCormack scheme, all physical variables are defined by the same calculating point and asymmetrical space difference is carried out in each step of difference. Therefore, if the fractional volume in each lattice shown in Fig. 4 is used, since the distance between calculating points in each step changes, introduction of the Favor method is difficult. In view of this, in this study, in order to introduce the Favor method, the fractional volume from arbitrary calculating point to the calculating point of each axial direction is calculated by Eq. 7 in simple. A backward difference is applied in the predictor step and a forward difference is applied in the corrector step.

$$V_{xi,k} = \frac{1}{2}\left(V_{i+1,k} + V_{i,k}\right) \; ; \quad V_{zi,k} = \frac{1}{2}\left(V_{i,k+1} + V_{i,k}\right) \tag{7}$$

where V_x and V_z = fractional volume in the x- and z-direction; and i and k = grid points in the x- and z-direction.

The following finite difference equations are written for Eq. 6:

[Predictor step]

$$U^P_{i,k} = U_{i,k} - \frac{\Delta t}{\Delta x \cdot V_{xi-1,k}}\left\{\left(E_{i,k} - E_{i-1,k}\right) - \left(A_{xi,k}Q_{xi,k} - A_{xi-1,k}Q_{xi-1,k}\right)\right\} - \frac{\Delta t}{\Delta z \cdot V_{zi,k-1}}\left\{\left(G_{i,k} - G_{i,k-1}\right)\right\} + \Delta t \cdot C_{i,k} \tag{8}$$

[Corrector step]

$$U^C_{i,k} = \frac{1}{2}\left(U_{i,k} + U^P_{i,k}\right) - \frac{1}{2}\frac{\Delta t}{\Delta x \cdot V_{xi,k}}\left\{\left(E^P_{i+1,k} - E^P_{i,k}\right) - \left(A_{xi+1,k}Q^P_{xi+1,k} - A_{xi,k}Q^P_{xi,k}\right)\right\} - \frac{1}{2}\frac{\Delta t}{\Delta z \cdot V_{zi,k}}\left\{\left(G^P_{i,k+1} - G^P_{i,k}\right)\right\} + \frac{1}{2}\Delta t \cdot C^P_{i,k} \tag{9}$$

where Δt = calculation time; Δx and Δz = grid size in the x- and z-direction; P and C = value in the predictor and corrector step; and Q = artificial viscosity term.

The artificial viscosity term Q of the x-direction is denoted by the following equation, while that of the z-direction is ignored because the artificial viscosity in the z-direction becomes large.

$$Q_{xi,k} = \frac{Kv}{8}\left(U_{i+1,k} - 2U_{i,k} + U_{i-1,k}\right) \tag{10}$$

where Kv = artificial viscosity coefficient.

The flow velocity of the z-direction w is calculated from Eq. 1 using a finite difference method under the boundary condition $w = 0$ at the bed. Moreover, in this study, we consider the pressure distribution in the vertical direction and calculate the pressure p after dividing into it the static pressure p_0 ($= \rho g(\xi - z)$; ξ = water surface elevation from a datum plane) and the anomaly pressure p'. The anomaly pressure p' is calculated from the Eq. 3 using a finite difference method under the boundary condition $p' = 0$ at the water surface. By means of this method, we apply a backward difference to the advection term and central difference to the others.

Boundary Conditions and Calculation Process

On the open boundaries, discharge is given at the upstream end and the measured flow depth is given at the downstream end. On the soil wall boundaries, friction by the log-law is given and there is no flux crossing through the wall. A free-slip condition is implemented at the water surface. In the initial condition, the downstream end depth is raised, and $u = \overline{u}$, $w = 0$, $p' = 0$ and ξ = constant are given in all calculating points. Then, the calculation process is carried out (1) by calculating the fractional volume and area in all lattices, (2) by calculating w, (3) by calculating p', (4) by calculating u and h, and these (1) - (4) are repeatedly calculated until the set time, reducing the flow depth of the downstream end gradually.

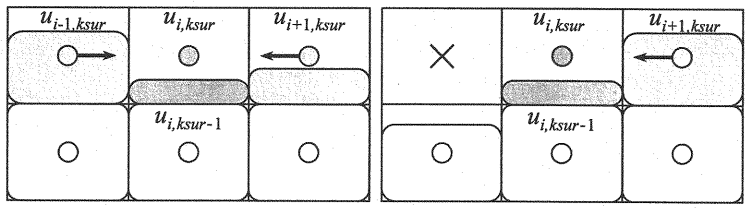

(a) Flowing from both sides (b) Flowing from one side

: New mesh

: The mesh in which the inflow velocity to the new mesh exists

Fig. 5 Handling of the new mesh in the water surface boundary after modeling

In this study, the water surface form in the lattice is modeled by the flat plane, as shown in Fig. 5, and the fractional volume and area in this lattice is calculated from the flow depth obtained for every time step. Therefore, when the flow depth increases, a new mesh is generated at the water surface boundary. At this time, it is necessary to assume the flow velocity of this new mesh, and since a free-slip condition is applied at the water surface, the flow velocity equal to it in the mesh under one is usually given. However, as shown in Fig. 5, when the flow velocity which flows into the new mesh exists, it is given by Eq. 11 in the case of (a), and it is given by Eq. 12 in the case of (b).

$$u_{i,ksur} = \left(u_{i+1,ksur} + u_{i-1,ksur}\right)/2 \tag{11}$$

$$u_{i,ksur} = \left(u_{i,ksur-1} + u_{i-1,ksur}\right)/2 \tag{12}$$

where $ksur$ = grid number of the new mesh in the z-direction.

The Minimum Fractional Volume

In a boundary lattice in which the fractional volume V will be in the state of $0.0 < V < 1.0$, the calculation diverges when V is in the state of $V \fallingdotseq 0.0$. So, in this study, when the fractional volume V is in the state of $V < V_{min}$, it is calculated as $V = 0.0$. V_{min} is the minimum fractional volume. Then, we carried out the calculation for estimating the V_{min} in an open channel. The open channel was a straight channel whose channel slope was 1/100, Manning roughness was 0.035, unit discharge was 83.3 cm^2/s and uniform flow depth was 3.01 cm, and we set up the V_{min} from the error between the uniform flow depth and the calculated one. The calculating conditions are $\Delta t = 0.001$ sec, $\Delta x = 2.0$ cm and $\Delta z = 0.5$ cm. Consequently, the error also became small so that the V_{min} was made small, and $V_{min} = 20$ % ($\Delta z \times V_{min} = 0.1$ cm) is adopted here so that the mean error was about 0.3 % and was sufficiently accurate for the present calculation.

Model Application

The calculation is performed for the experiment carried out by Suzuki et al (12). The experimental and the calculating conditions are shown in Table. 1. The calculation domain is fixed with 250 cm length in the x-direction and 25 cm height in the z-direction, and the back-ward facing step is installed at the position of 50 cm in the downstream direction from the upstream end. The difference between generating conditions of each flow (the wave jump and the submerged jet) is based on the difference of the flow depth at the downstream end. Moreover, as for the artificial viscosity coefficient Kv, since the solution becomes dull if Kv is enlarged, the smallest values among Kv which were able to obtain the solution without calculation diverging in preliminary calculation are given.

Table. 1 Experimental and calculating conditions

Bed slope I	1/300	Δt (sec)	0.001
Manning roughness n	0.017	Δx (cm)	2.0
Step height W (cm)	10	Δz (cm)	0.5
Unit discharge q (cm^2/s)	400	Artificial viscosity coefficient Kv	1.5
Flow depth at downstream end h_t (cm)	Wave jump : 13.78, Submerged jet : 10.92		

RESULTS AND DISCUSSION

Calculation of the Wave Jump

In order to compare the experimental results with the calculated ones in the state of the wave jump, (a) the experimental result of the flow velocity contour, (b) the calculated result of the flow velocity contour and (c) the calculated results of the flow velocity vectors at 60 seconds after calculations were started are shown in Fig. 6. In the experimental results, the main flow after leaving the step flows along the water surface and the flow width is diffused gradually. The maximum flow velocity of the main flow exists near the water surface after leaving the step, and it is concentrated especially on the place where the water surface has curved downward. The calculated results reproduce the flow velocity and the water surface form well.

The change of the maximum water surface evolution in every second by repetition of calculation is shown in Fig. 7. "Flow depth at the downstream end is fixed" in this figure means that the flow depth reached the designated flow depth since the flow depth was gradually lowered from the state of afflux in this calculation. From this figure, the flow did not reach in a stationary state even if the time is 60 seconds after. Moreover, the time change of the water level at 300 seconds after is shown in Fig. 8, and it was found that the flow did not reach a stationary state (see Nakamoto et al. (9)) also from this figure. It is thought that this is due to the repetition of collapse and formation of the wave form at the wave crest. Although not shown in a figure, the reason for this is that the generating position of the maximum water surface evolution was concentrated on the wave just behind the step and the downstream end depth h_t was near the flow shift condition (from the wave jump to the submerged jet). In fact, it has been observed also in the experiment (Suzuki et al. (12)) that it is very unstable flow by which the collapse and formation of the wave crest are repeated near the flow shift condition. Thus, the result at 60 seconds after the calculation start shown in Fig. 6 is the result when the flow is still in an unstable state.

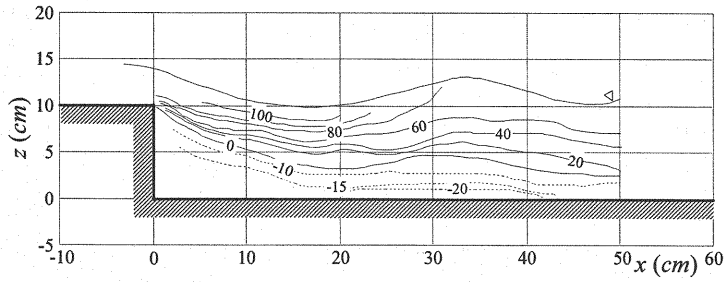

(a) Flow velocity contour (experiment)

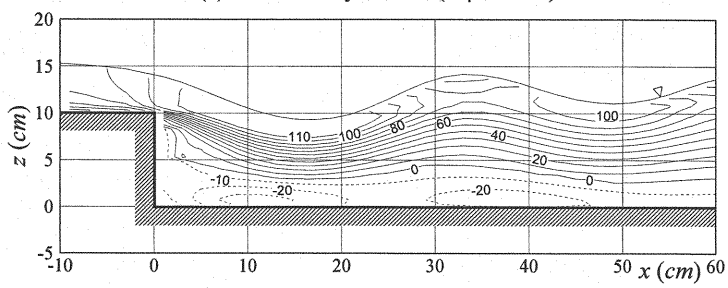

(b) Flow velocity contour (calculated)

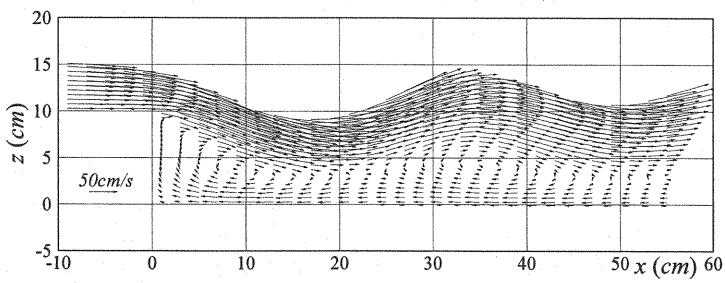

(c) Flow velocity vectors (calculated)

Fig. 6 Comparison between measured and calculated wave jump

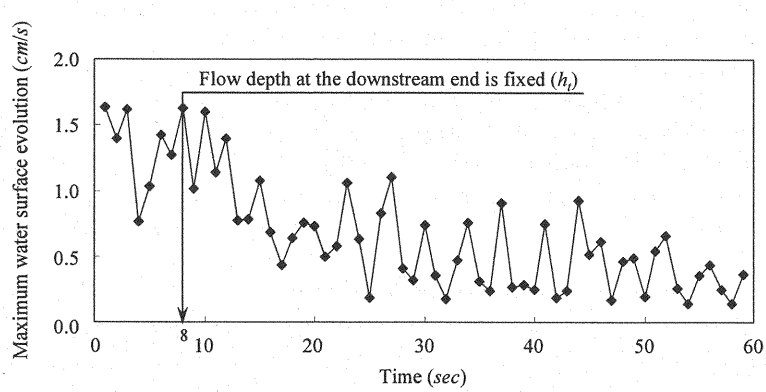

Fig. 7 Change of the maximum water surface evolution by repetition of calculation (wave jump)

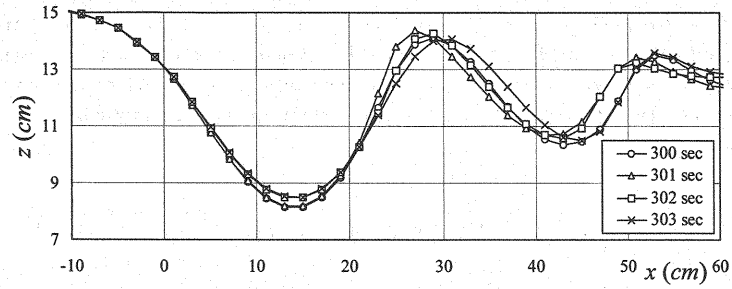

Fig. 8 Time change of water level (wave jump)

Calculation of the Submerged Jet

Fig. 9 shows the experimental results and the calculated results (at 60 seconds after) of the submerged jet. Findings reveal that, the main flow after leaving the step impinges on the bed keeping the flow width, and flows along the bed expanding the flow width gradually. The roller of reverse flow is formed near the water surface just behind the step, and the water surface form is in the comparatively flat state. Also, in the calculated result, the roller of reverse flow is formed near the water surface, and the main flow flows along the bed. The calculated results reproduce the flow characteristic of the submerged jet well.

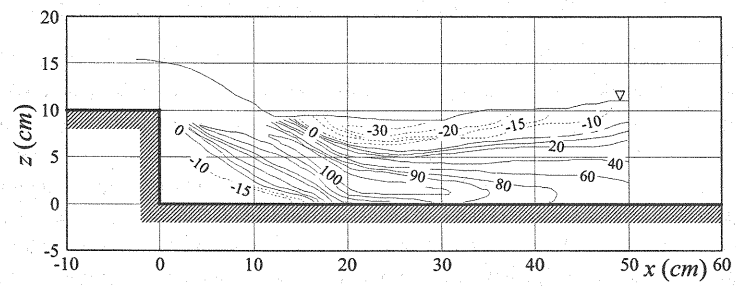

(a) Flow velocity contour (experiment)

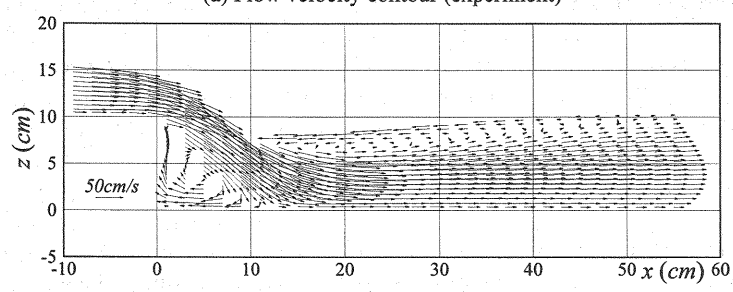

(b) Flow velocity contour (calculated)

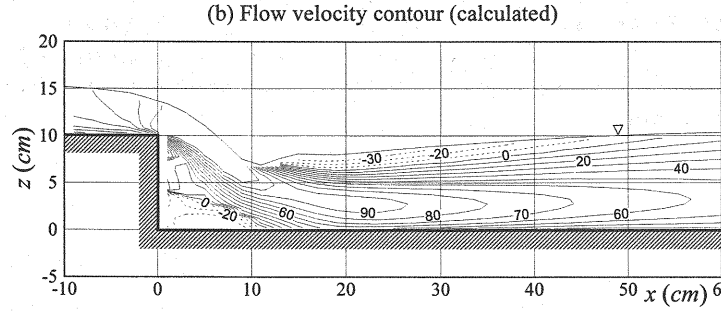

(c) Flow velocity vectors (calculated)

Fig. 9 Comparison between measured and calculated submerged jet

The change of the maximum water surface evolution in every second in the state of the submerged jet is shown in Fig. 10. This figure shows that the flow has reached a stationary state mostly at 30 seconds after. It was concluded from this, the water surface in the state of submerged jet by calculation is calm, and the reason why the water surface form becomes comparatively flat in the experiment can be understood.

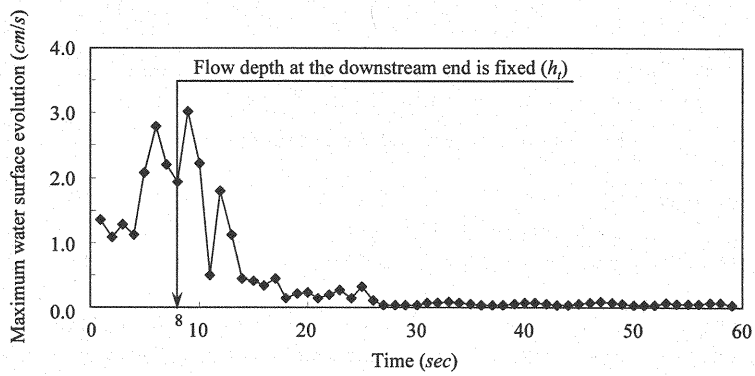

Fig. 10 Change of the maximum water evolution by repetition of calculation (submerged jet)

The Shift Process

In this section, reproducing calculation about the shift process of each flow (the wave jump and the submerged jet) is tried by operating the downstream end depth h_t under the condition used until now. The downstream end depth h_t is changed up and down in the 11 - 16 cm range. In regard to the operating speed of the downstream end depth, since it is thought that the operating speed is related to the shift condition of each flow shown in next paragraph, we calculated in the 0.05 - 0.2 cm/s range regarded as smaller than the operating speed in experiment in preliminary calculation. Consequently, since the influence on the shift limit by the size of operating speed hardly appeared, we adopted 0.1 cm/s in our study.

The velocity vectors of the shift process from the wave jump to the submerged jet are shown in Fig. 11, and ones of the shift process from the submerged jet to the wave jump are shown in Fig. 12. First, when the flow shifts to the submerged jet from wave jump, the wave form begins to appear more notably as the downstream end depth is reduced gradually (Fig. 11 - (b)). Then, the moment the flow shifts to the submerged jet from the wave jump, the wave crest changes into a state which resembles the wave-breaking toward the upstream, and the roller of reverse flow begins to be formed on the water surface (Fig. 11 - (c), (d)). Finally, the main flow begins to flow along the bed so that it may be crushed by the roller of reverse flow (Fig. 11 - (e)). On the other hand, when the flow shifts to the wave jump from the submerged jet, the reverse flow field also becomes large with each increase in the downstream end depth, and the reattachment point position of the main flow moves toward the downstream from near the step (Fig. 12 - (a), (b)). Then, the main flow separates from the bed at a certain moment, and the reverse flow field is flushed by that flow in an instant (Fig. 12 - (c), (d)).

Since these shift processes of each flow are similar with a flow of a falling works with a trench in the experiment by Fujita et al. (2), it is thought that the numerical model can reproduce the shift process of each flow over backward-facing step well.

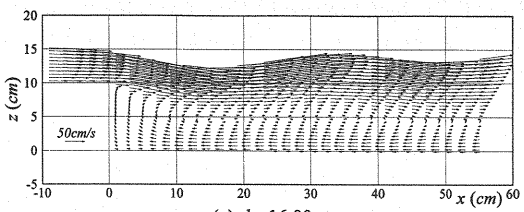

(a) h_t=16.00 cm

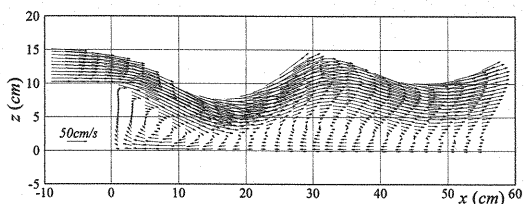

(b) h_t=13.80 cm

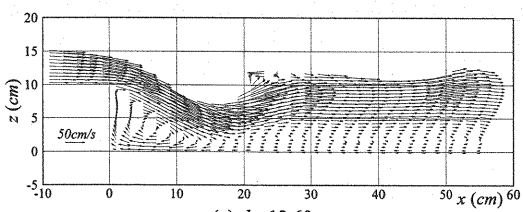

(c) h_t=13.60 cm

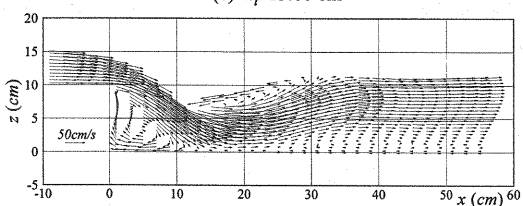

(d) h_t=12.90 cm

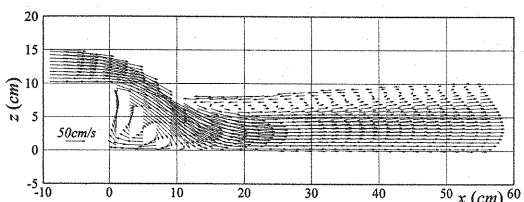

(e) h_t=11.00 cm

Fig. 11 The wave jump to the submerged jet

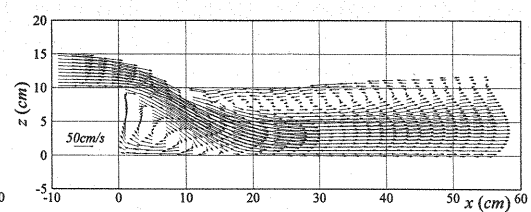

(a) h_t=12.90 cm

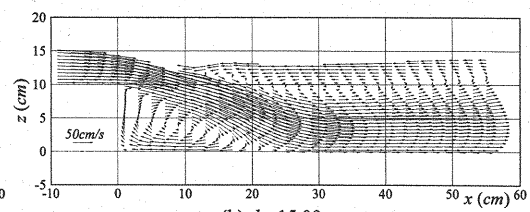

(b) h_t=15.00 cm

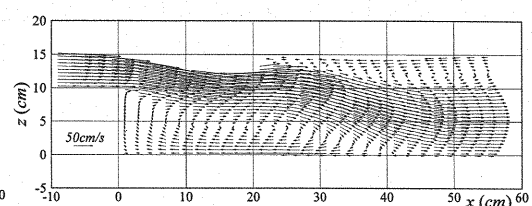

(c) h_t=15.60 cm

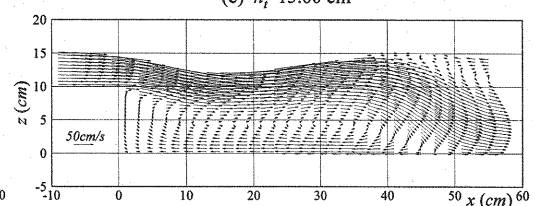

(d) h_t=15.70 cm

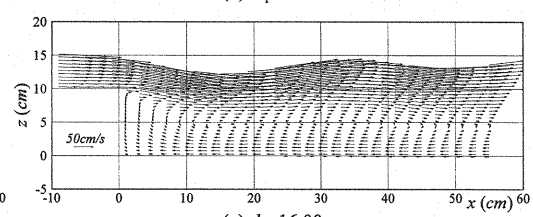

(e) h_t=16.00 cm

Fig. 12 The submerged jet to the wave jump

Calculation of the Shift Condition

In this section, a comparison with the experimental results and the calculated ones about the shift condition of each flow is carried out. First, the critical state is explained. In measurement of the shift condition in experiment, when the flow shifts to the submerged jet from the wave jump, the water surface slope in just downstream of the backward-facing step becomes large by reducing the downstream end depth, and the state of the flow becomes unstable. This condition is regarded as the critical condition of the wave jump. Conversely, when the flow shifts to the wave jump from the submerged jet, the flow changes the wave jump from the submerged jet by raising the downstream end depth in an instant. This condition is regarded as the critical

condition of the submerged jet. Thus, in the calculation, the unstable state of Fig. 11 - (b) or (c) is regarded as the shift condition from the wave jump to the submerged jet, and the state of Fig. 12 - (c) or (d) is regarded as the shift condition from the submerged jet to the wave jump. In the experiment, the step height W is 4.5 - 11.5 cm, and the unit discharge q is changed in 50 - 500 cm^2/s range. In the calculation, W is in 5 - 15 cm and q is changed in 250 - 500 cm^2/s ranges almost similarly. And the downstream end depth h_t is fluctuated in the 0.1 cm/s.

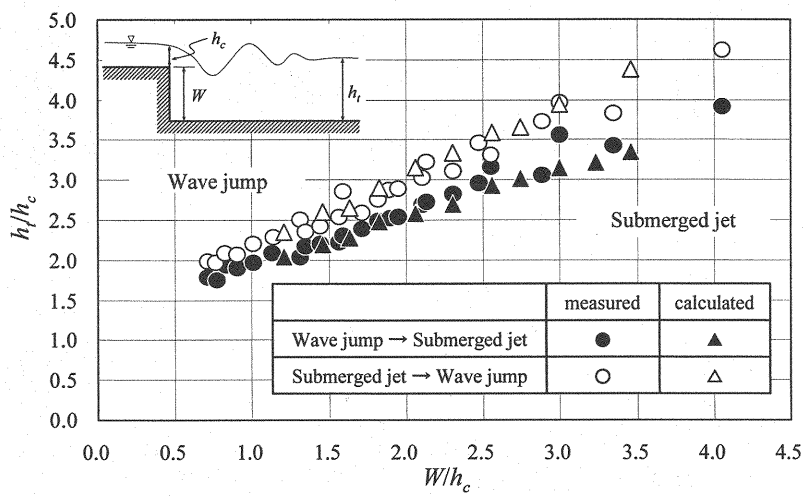

Fig. 13 Comparison of between measured and calculated shift condition

A comparison between the measured and calculated shift condition is shown in Fig. 13. h_c is the critical depth in each discharge conditions, and the horizontal axis W and the vertical axis h_t are divided by the critical depth h_c. From this figure, the calculated results can be seen to be in good agreement with the experimental ones for the both of shift conditions, and this reproduces the tendency where the shift condition also becomes large as the step height W becomes large under the fixed discharge condition.

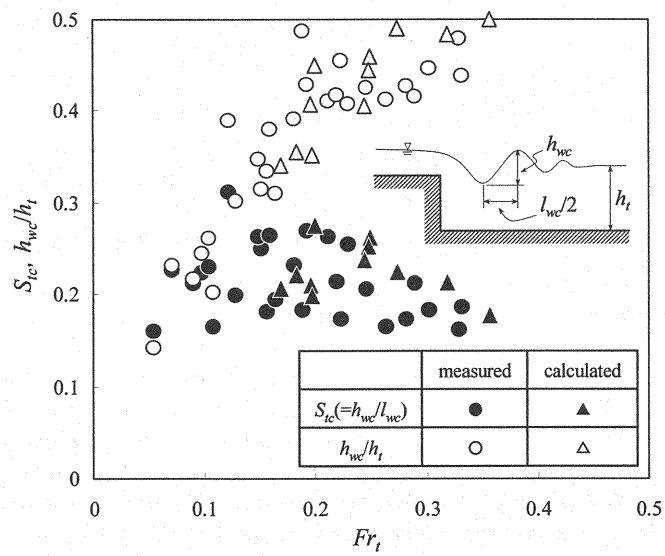

Fig. 14 Comparison of between measured and calculated wave height

The relation between the Froude number at the downstream end Fr_t, the ratio of the wave height to length S_{tc} and the wave height h_{wc}/h_t in case the flow shifts to the submerged jet from the wave jump is shown in Fig. 14. In the experiment, it is reported that the ratio of the wave height to length S_{tc} becomes about 0.2 ~ 0.3 when the flow is close to the shift condition, and the h_{wc} will be about 0.5 times the h_t although the wave height h_{wc}/h_t increases with the increase of the Fr_t. In these points, the calculated result shows almost the same value and tendency as experimental one, so it is thought that this numerical model is able to reproduce well the wave form at the time of the shift condition.

CONCLUSIONS

In this study, a 2-dimensional vertical numerical model, which employs the MacCormack scheme and is based on the Favor method for the governing equations, has been developed; and a complex flow over backward-facing step was calculated by means of this numerical model. The calculation of the wave jump, the wave form of the water surface and the flow velocity were reproduced well. Furthermore, the unstable flow near the flow shift condition was also reproduced. As for the calculation of the submerged jet, the flow which includes the characteristic roller of reverse flow near the water surface was reproduced well. Moreover, for the calculation of the shift process of each flow (the wave jump and the submerged jet), this model could reproduce the phenomena where the wave crest changes into a state which resembles wave-breaking when shifting to the submerged jet from the wave jump. The main flow flushes the reverse flow field when shifting the wave jump from the submerged jet, and the shift condition. In the future, a movable bed numerical model will be introduced so that it can be applied to local scouring at the downstream areas of consolidation works.

REFERENCES

1. Blom, M.P. : Numerical modeling of local-scour holes using k-ε turbulence-model, JSCE, Vol.51/II-58, pp.116-117, 1996.
2. Fujita, I. and T. Maruyama : Hydraulic characteristics of open-channel flow downstream of a falling works with a trench, Ann. Jour. of Hydraulic Eng., JSCE, Vol.45, pp.403-408, pp403-407, 2001 (in Japanese).
3. Hirt, C.W. and J.M. Sicilian : A Porosity Technique for the Definition Obstacle in Rectangular Cell Meshes, Flow science, Inc. Los Alamos, New Mexico, pp.450-469, August 1985.
4. Hirt, C.W. : Volume-Fraction Techniques, Powerful Tools for Wind Engineering, Proc. First Int. Symp. on Comp. Wind Eng., pp.333-344, Tokyo, 1992.
5. Kanda, K., Muramoto, Y. and Y. Fujita : Scour process and flow characteristics in downstream of bed protection works, Disaster Prevention Research Institute Annuals, Kyoto University, Vol.36, No.B-2, pp.551-569, 1993 (in Japanese).
6. Kurniawan, A., Altinakar, M.S. and W.H. Graf : Flow pattern of an eroding jet, XXIX IAHR Congress Proceedings, Theme D Vol.1, pp.390-396, Beijing, China, 2001.
7. Liu Yu-Ling : Study of The Mathematical Model for Numerical Solution of Supercritical Surface Flows, XXIX IAHR Congress Proceedings, Theme D Vol.1, pp.390-396, Beijing, China, 2001.
8. Michiue, M. and K. Suzuki : Study of the hydraulic functions of the consolidation work across the river, Disaster Prevention Research Institute Annuals, Kyoto University, Vol.22, No.B-2, pp.507-519, 1979 (in Japanese).
9. Nakamoto, H., Michiue, M. and O. Hinokidani : A numerical analysis of a complex flow over the back-ward facing step, JSCE, Vol.55/II-344, 2000 (in Japanese).
10. Nakayama, A. and S. Yokojima : Turbulence model with free-surface fluctuation effects for the calculation of open-channel flows, Ann. Jour. of Hydraulic Eng., JSCE, Vol.43, pp.389-394, 1999 (in Japanese).
11. Ohtsu, I. and Y. Yasuda : Characteristics of flow over drop structure, Proceeding of International Conference on Hydraulics in Civil Engineering, University of Queensland-Brisbane, Australia, pp.223-228, 1994.
12. Suzuki, K., Michiue, M., and O. Hinokidani : Flow properties downstream of a sill, Proceedings of the 29th Japanese Conference on Hydraulics, pp.615-620, 1985 (in Japanese).

APPENDIX - NOTATION

The following symbols are used in this paper:

A_x, A_z	=	fractional area in the x- and z- direction;
F_{rt}	=	Froude number at the downstream end;
g	=	gravity acceleration;
h	=	flow depth;
h_c	=	critical depth;
h_t	=	flow depth at downstream end;
h_{wc}/h_t	=	wave height;
i, k	=	grid points in the x- and z-direction;
I	=	bed slope;
$ksur$	=	grid number of the new mesh in the z-direction;
Kv	=	artificial viscosity coefficient;
n	=	Manning roughness;
p	=	pressure ($= p_0 + p'$);
p_0	=	static pressure ($= \rho g(\xi - z)$);
p'	=	anomaly pressure;
P, C	=	value in the predictor and corrector step;
q	=	unit discharge;
Q	=	artificial viscosity term;
S_{tc}	=	ratio of the wave height to length;
u, w	=	velocity in the x- and y-direction;
u_*	=	shear velocity;
V	=	fractional volume;
V_{min}	=	minimum fractional volume;
V_x, V_z	=	fractional volume in the x- and z-direction;
W	=	step height;
x, z	=	horizontal and vertical axis of the coordinate;
z'	=	zero at the bed level and positive upper in the vertical direction;
Δx, Δz	=	grid size in the x- and z-direction;
Δt	=	calculation time;
ε_h, ε_z	=	eddy viscosity coefficient in the horizontal and vertical direction;
κ	=	Von Karman constant (= 0.41);
ξ	=	water surface elevation from a datum plane;
ρ	=	water density; and
$\bar{}$	=	depth averaged values.

(Received June 30, 2003 ; revised October 8, 2003)